## LANGMUIR

pubs.acs.org/Langmuir Article

# Investigation of Ultramicroporous Structure of One-Dimensional Lepidocrocite Titanates Using Carbon Dioxide and Nitrogen Gases

Akimaro Yanagimachi,\* Takayuki Kono, Kota Ota, Takeshi Torita,\* Daja R. Bonilla, Daniel E. Autrey, Hussein O. Badr, and Michel W. Barsoum\*



Cite This: https://doi.org/10.1021/acs.langmuir.4c01689



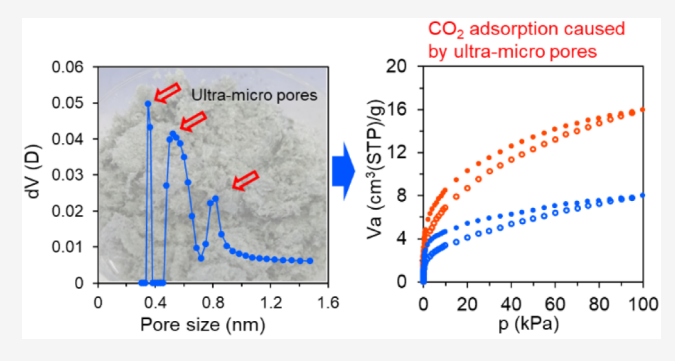
**ACCESS** I

III Metrics & More

Article Recommendations

s Supporting Information

ABSTRACT: The novel material, one-dimensional lepidocrocite (1DL) titanate, is attracting industrial and scientific interest because of its applicability to a wide range of practical applications and its ease of synthesis and scale up of production. In this study, we investigated the CO<sub>2</sub> adsorption capability and pore structures of 1DL freeze-dried and lithium chloride washed air-dried powders. The synthesized 1DL was characterized by X-ray diffraction, Raman spectroscopy, and scanning electron microscopy. Using the constant-volume method, CO<sub>2</sub> gas adsorption revealed that the 1DL exhibits type IV adsorption—desorption isotherms. The heats of adsorption obtained from the adsorption branches are lower than those obtained from the desorption branches. Brunauer—



Emmett–Teller (BET) analysis, using  $N_2$  gas adsorption isotherms at 77 K showed that 1DL possesses 80.2 m<sup>2</sup>/g of BET specific surface area. Nonlocal density functional theory analysis indicated that two types of pores, meso-pores and ultramicro pores, exist in the 1DL freeze-dried powders. This work provides deep insights into the pore structures and  $CO_2$  adsorption mechanisms of 1DL powders.

#### INTRODUCTION

Global warming, caused by the escalating emission of the greenhouse gas carbon dioxide (CO<sub>2</sub>), has become a worldwide crisis.<sup>1</sup> Human activities, particularly the combustion of fossil fuels (such as coal, oil, and natural gas) and deforestation, are responsible for CO<sub>2</sub> emissions. In response to this pressing issue, extensive international endeavors have been undertaken. A notable instance is the adoption of the Paris Agreement in 2015. Furthermore, Japan has proclaimed its commitment to achieve carbon neutrality–effectively eliminating net CO<sub>2</sub> emissions—by the year 2050.<sup>2</sup>

To mitigate the environmental impact of  $CO_2$ , various measures aimed at emission reduction and recovery have been implemented.<sup>3,4</sup> Among these measures,  $CO_2$  capture is a crucial process for the effective utilization of  $CO_2$ . If captured  $CO_2$  can be used for enhanced oil recovery,<sup>5</sup> it could be sequestered underground for a long time. It would also allow for the conversion of  $CO_2$  into value-added materials,<sup>6</sup> and it could also be used to boost the growth of plants in greenhouses,<sup>7</sup> among many other applications.  $CO_2$  can also be fixed by  $CO_2$  mineralization. Mineralized  $CO_2$  can be stably discarded into the underground.<sup>8</sup>

The list of materials that have been proposed to capture  $CO_2$  is long. Among these, MXenes are recognized for their capacity to adsorb  $CO_2$  both on their surfaces and within their interlayer spacings. Additionally, MXenes exhibit photo-

catalytic activity that facilitates the conversion of CO<sub>2</sub> into valuable materials. <sup>10</sup> Another noteworthy group of adsorbents is metal—organic frameworks (MOFs), which demonstrate the ability to adsorb CO<sub>2</sub>. Specifically, MOFs constructed from cyclodextrin and metal ions exhibit enhanced selectivity in adsorbing CO<sub>2</sub> from CO<sub>2</sub>/C<sub>2</sub>H<sub>2</sub>/He mixtures, resulting in their increased concentration. <sup>11</sup> Notably, this particular type of MOF experiences changes in conductivity upon CO<sub>2</sub> adsorption, rendering it a promising candidate for novel CO<sub>2</sub> sensors. <sup>12</sup> Other adsorbents characterized by high specific surface areas, such as molecular sieves and activated carbon, also effectively adsorb CO<sub>2</sub>. <sup>13,14</sup>

Titania,  $TiO_2$ , and  $TiO_2$ -based materials such as titanates, have also shown potential as effective  $CO_2$  adsorbents. It is known that  $TiO_2$  adsorbs  $CO_2$ . and several studies including surface modification and making composites with other materials, making particle size nano-order have been performed to enhance the  $CO_2$  capturing capacity of  $TiO_2$ .

Received: May 6, 2024 Revised: July 3, 2024 Accepted: July 3, 2024 Published: July 17, 2024



Recently, we discovered a simple, single pot, scalable method to make a truly one-dimensional, 1D,  ${\rm TiO_2}^{20}$  Because the structure is that of lepidocrocite, we refer to this new form of  ${\rm TiO_2}$  as 1DL.  $^{21-23}$  Using a combination of X-ray diffraction, XRD, and high resolution transmission electron microscope (HRTEM) images, we concluded that the 1DL are nanofilaments (NF) 5  $\times$  7 Ų in minimum cross-section and tens of nanometers in length.  $^{21,24}$  Figure 1A shows a schematic of a

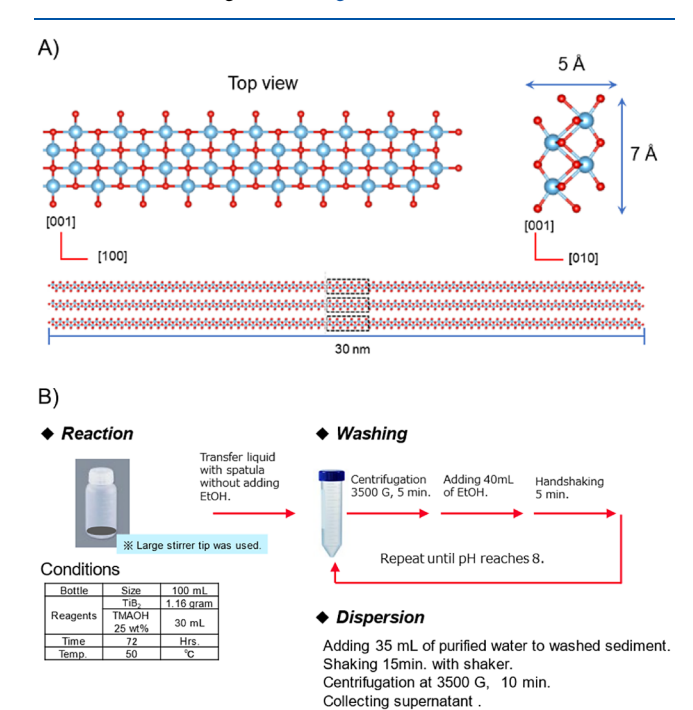


**Figure 1.** 1DL structure and synthesis procedure. A) Structure showing minimum cross-section of  $2 \times 2$  TiO<sub>6</sub> octahedra and a high aspect ratio along the growth direction; maximum width is a 2D flake. B) Synthesis procedure.

single 1DL comprised of  $2 \times 2$  edge shared TiO<sub>6</sub> octahedra. The latter grow in the *a*-direction and self-assemble in the *b*-direction. The lengths of these 1DLs are in the 20 to 50 nm range, which implies that their aspect ratios are of the order of 60 (see bottom sketch in Figure 1A). One gram of 1DL spans 400 million miles and covers  $\approx 2,000 \text{ m}^2.25$ 

It is important to note here that claims of 1D titania are numerous.  $^{26-31}$  Our 1DLs, however, are the only ones that meet the quantum mechanical definition of 1D in that their band gap energy,  $E_g$ , is subject to quantum confinement. At 4 eV,  $E_g$  of dilute 1DL suspensions is 4 eV. This record value for titania is due to quantum confinement along two dimensions. At  $\approx 3.2$  eV,  $E_g$  for bulk anatase and rutile are considerably lower. Thus, it is not surprising that the electronic band structures of 1DL and anatase/rutile are different.  $^{32}$ 

1DL synthesis is surprisingly simple: We react, Ti-containing compounds like TiB<sub>2</sub>, TiC, etc., with tetramethylammonium hydroxide (TMAOH) in the 50 to 90 °C temperature range under 1 atm. for tens of hours, h. This results in the 1DL shown in Figure 1A. After washing with ethanol, EtOH, to  $\approx$  pH 7, the final morphology one obtains is a sensitive function of how the 1DLs are further processed. If water is used, a stable colloid is formed. Filtering the colloid suspension results in what appears to be 2D layers. The layers, however, are comprised of 1DLs self-assembled into sheets that we label

quasi-2D or q-2D. An impetus of this work was our realization that the 1DLs self-assemble in multiple configurations.

After synthesis and washing with EtOH to pH 7, the interfilamentous space is occupied by TMA cations, TMA $^+$ . The latter can be readily ion exchanged by other cations such as Li, H<sub>3</sub>O, Na, Mg, Mn, Fe, and Ni, among other mono and divalent cations etc. <sup>30,33</sup> For instance, Li-intercalated 1DLs can be exchanged by actinide cations such as U<sup>4+,24</sup>

We have already shown that 1DLs can be used for a large host of applications. They can be used as electrodes in lithiumion and lithium—sulfur batteries, <sup>21,34</sup> photochemical hydrogen production, <sup>35</sup> chemical cancer therapies, <sup>21</sup> water purification, <sup>24</sup> dye degradation, <sup>25</sup> polymer composites, <sup>36</sup> and perovskite solar cells. <sup>37</sup>

Compared to the other  $CO_2$  capturing materials, the 1DLs have several advantages. First, the processing is simple, one pot, and easily scalable. Currently, in the lab, we can make 100 g of 1DL per batch under ambient pressure. Second, the 1DL are synthesized from relatively inexpensive nontoxic earth abundant materials such as  $TiB_2$  and TiC. The third is theoretical specific surface area >1500 m<sup>2</sup>g<sup>-1</sup>.

The purpose of this work is to report the  $CO_2$  capturing ability of our 1DL for the first time. In doing so we shed important light on the pore sizes and their distribution.

We worked with porous powders prepared by freeze-drying, FD, and other methods after replacing the TMA $^+$  with lithium by washing with a lithium chloride (LiCl) solution and airdrying. We confirmed that LiCl washing decreases distance between 1DLs, as reported previously. We also document, for the first time, that 1DL powders possess ultramicro pores. The finding will expand their applicability to the gas molecule adsorption field. Furthermore, we confirmed that distance between 1DLs also decreases after degassing at 200 °C followed by  $\rm CO_2$  adsorption desorption process also for the first time.

### EXPERIMENTAL AND COMPUTATIONAL METHODS

Figure 1B summarizes the synthesis procedure. First, 1.16 g of TiB<sub>2</sub> (Kojundo Chemical Laboratory Co., Ltd.) and 30 mL of 25 wt % TMAH in water (Tokyo Chemical Industry Co., Ltd.) were added to a 100 mL wide-mouth bottle (AS ONE Corp., Japan). Next, a magnetic stirrer tip whose diameter (35 mm) was similar to the bottom of the bottle was added. The system was then heated to 50  $^{\circ}\text{C}$ using a water bath for 72 h while vigorously stirring. After 72 h, the entire mixture was transferred to a 50 mL centrifuge tube. The mixture was centrifuged at 3500 G for 5 min to separate the sediment from the supernatant. After centrifugation, the latter was discarded, and 40 mL of 99.5% EtOH, (FUJIFILM Wako Pure Chem. Corp.) was added to the remaining sediment in the centrifuge tube. The latter was hand-shaken for 5 min to disperse the sediment. The centrifugation and hand-shaking cycles were repeated (usually 3 times) until the pH of the solution was <8.0. In all cases, the supernatant was discarded. The last step was the addition of 35 mL of DI water to the sediment. The mixture was shaken with an automatic shaker (Fast and Fluid Management B. V.) for 15 min before centrifugation at 3500 G for 10 min. The supernatant, comprised of a 1DL colloid suspension, was collected. Henceforth, these samples made will be referred to the colloid.

One milliliter of 1DL colloid and 20 mL of DI water were mixed and shaken with an automatic shaker for 5 min. The liquid was vacuum filtered into a film using a membrane filter (pore size: 0.22  $\mu$ m, Durapore, Merck Millipore). Henceforth, these samples will be referred to as filtered films, FFs.

Another fraction of the 1DL colloid was frozen to  $-38\,^{\circ}\mathrm{C}$  using a medical freezer (FMF-038F1, FUKUSHIMA GALILEI Co., Ltd. Japan). The frozen colloid was then freeze-dried to obtain a powder that will henceforth be referred to as FD.

In another set of experiments, 1DLs were prepared and dried in open air at 50 °C overnight, and then tested as synthesized (i.e., without freeze-drying). In this case, 10 g of TiB2 precursor powders (-325, Thermo Scientific, PA) were mixed with 100 mL of 25 wt % TMAH aqueous solution (Electronic grade, 99.9999%, Alfa Aesar, PA) in a 250 mL wide-mouth plastic bottle. Two fine needles were inserted into the bottle to avoid pressure buildup during the reaction. The mixture was shaken at 80 °C for 120 h using a temperaturecontrolled shaker (Labnet 211DS, 49L, 120 V, NJ) under atmospheric pressure. After the reaction, the resulting powders were combined with ~200 mL ethanol (Decon Lab Inc., 200 proof, PA) in a beaker (1L in volume), stirred for 1-2 h using an overhead mixer, and the mixture was allowed to settle. The supernatant was discarded as chemical waste. This washing step was repeated multiple times until the pH reached 7. To exchange TMA+ with Li+, 200 mL of 5 M LiCl solution (LiCl, Anhydrous, 99%, 20 mesh, Alfa Aesar, PA) was added to the powders and stirred using an overhead mixer for 1-2 h under ambient conditions. This step was performed three subsequent times to ensure full cation exchange. The powders were then rinsed with DI water (Millipore, 18.2 M $\Omega$ , TOC < 3 ppb) for 3 cycles to remove any unreacted LiCl salt or reaction byproducts. Finally, the resulting particles were allowed to dry overnight at 50 °C in open air. Henceforth, the resulting powder will be referred to as the LiCl airdried powder.

XRD diffraction, XRD, patterns of FD samples were obtained on a diffractometer (Smart Lab3, Rigaku). The source: X-ray was Cu  $\rm K_{\alpha}$  over the  $2^{\circ}$  to  $85^{\circ}$   $2\theta/\theta$  angular range. The step size was  $0.02^{\circ}$  and the time per step was 40 s. XRD patterns for the LiCl air-dried samples were acquired using a different diffractometer (Rigaku Miniflix, Tokyo, Japan) also using Cu  $\rm K_{\alpha}$  radiation at 40 kV and 15 mA. The powders were scanned in the  $2^{\circ}-65^{\circ}$   $2\theta$  range with a step size of  $0.02^{\circ}$  and a dwell time of 1 s.

Raman spectroscopy of the FD samples was performed on a spectrometer (RAMAN touch VIS-MA, nanophoton) using laser excitation with a wavelength of 532 nm and 220 kW/cm² powder density. To image the material, we used a scanning electron microscope, SEM (SU-5000, Hitachi HIGHTECH). The accelerating voltage was 5 kV and a secondary electron (SE) detector was used. To prepare samples for SEM, we drop cast the colloid on porous alumina substrates. We also used a scanning transmission electron microscope, STEM (JEOL JEM-F200/Noran system 7) to observe the structure of the material. The accelerating voltage was 200 kV.

Adsorption isotherms of LiCl air-dried samples with  $\rm CO_2$  as the adsorbate, were measured using a gas adsorption analyzer (Quantachrome Autosorb iQ-XR) equipped with a temperature-controlled recirculating Dewar to collect isotherms at 273, 278, 283, 288, and 293 K in the 0.017–100.7 kPa pressure range. Prior to the adsorption measurements, these powders were degassed under vacuum at 200 °C for 15 h. No outgassing between different isotherm temperatures was performed.

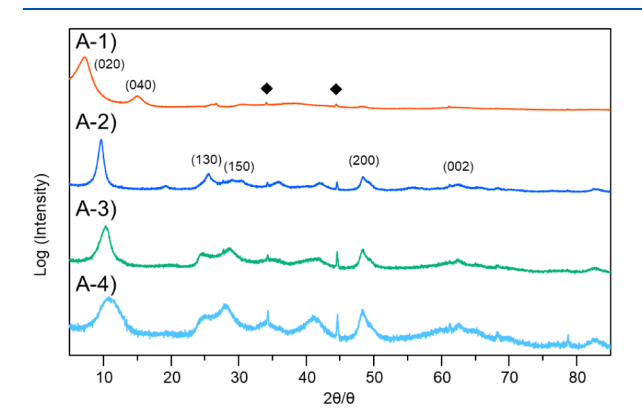
The pore-size distribution curves were calculated from the adsorption branch of the isotherm at 273 K by application of a nonlocal density functional theory (NLDFT) model assuming CO<sub>2</sub> adsorption at 273 K on a carbon adsorbent. Adsorption—desorption isotherms of FD samples with CO<sub>2</sub> at 298 and 353 K were obtained using a gas adsorption analyzer (BELSORP MAX, MicrotracBEL) in the 0.0006–100.15 kPa pressure range. Prior to the adsorption measurements, the FD samples were degassed under vacuum at 180 °C for 2 h.

Adsorption experiments of LiCl air-dried samples with nitrogen,  $N_2$ , as the adsorbate (77 K) were performed using a gas adsorption analyzer (Quantachrome Autosorb iQ-XR) in the 0.0008–100.15 kPa pressure range. Prior to the adsorption experiments, the LiCl air-dried samples were outgassed under vacuum at 200  $^{\circ}\text{C}$  for 15 h. The SSA was calculated using the  $N_2$  adsorption isotherm at 77 K using the Brunauer–Emmett–Teller (BET) method. The pore-size distribution

curves were calculated from the adsorption branch of the isotherm by application of a NLDFT method assuming  $N_2$  adsorption at 77 K on a silica substrate with cylindrical pores in the mesopore range.

#### ■ RESULTS AND DISCUSSION

Figure 2 plots, on a log scale, typical XRD patterns of the various powders tested here. In all cases, the peaks are indexed



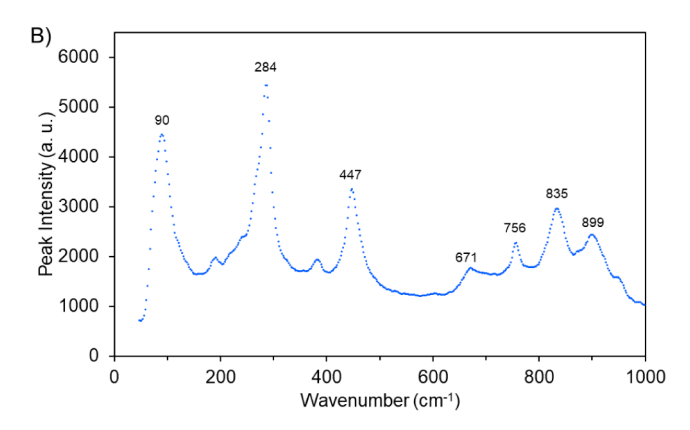


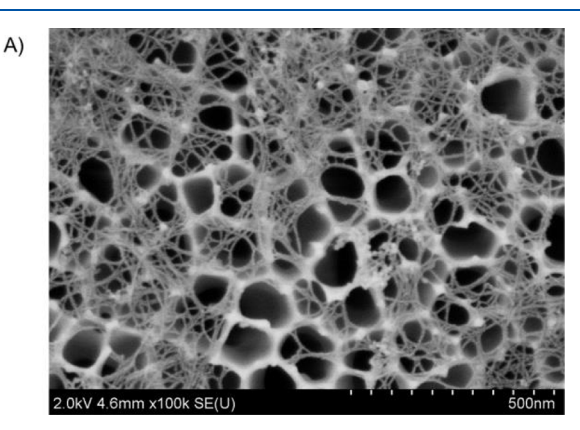
**Figure 2.** XRD and Raman characterization of various powders used herein. A-1) Typical XRD pattern of 1DL TiO<sub>2</sub> FD powder, A-2) LiCl washed air-dried, A-3) outgassed at 200 °C, and A-4) after  $\rm CO_2$  adsorption desorption. In all patterns sharp peaks belong to the  $\rm TiB_2$  precursor. B) Raman spectrum pattern of 1DL FD powder. All peaks belong to  $\rm TiO_2$  lepidocrocite.

and are quite similar to ones we have published previously.<sup>22</sup> In brief, there are 3 types of peaks. Low angle 0k0 peaks, viz. 020, 040, etc., that are measure the distance, d, between the filaments along the b-direction. Peaks at  $48^{\circ}$  and  $62^{\circ}$   $2\theta$ correspond to the 200 and 002 planes and are not a function of what is in between the 1DLs as observed here (Figure 2). From these peaks, we obtain a- and c-lattice parameters that are in excellent agreement with our previous work and, more importantly, with those for 2D lepidocrocite titanates.<sup>22</sup> The last set of planes is between the 0k0 and 48 $^{\circ}$  2 $\theta$  peaks. The locations of these peaks are weak functions of what is between the 1DLs and can be indexed as in 2D lepidocrocite (Figure 2). The peak shift with outgassing at 200 °C and exposure to CO<sub>2</sub>. would occur from the partial desorption of intercalated hydrated water. Previous DFT calculation results suggest that the interlayer distances are 9.87 and 6.45 Å for hydrated and unhydrated lithium, respectively.<sup>38</sup> Therefore, it is reasonable to assume that the partial desorption of hydrated water reduces

the interlayer distances in the interlayer distance range (9.87 Å to 6.45 Å). The weak sharp peaks are those of unreacted TiB<sub>2</sub>.

To further investigate the structure, Raman spectroscopy was carried out. The results (Figure 2E) are consistent with those of lepidocrocite  $TiO_2$ .

The SEM micrograph shown in Figure 3A, clearly shows the 1D nature of our material. Based on these results, we conclude



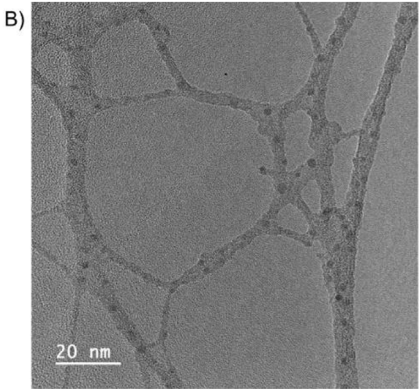
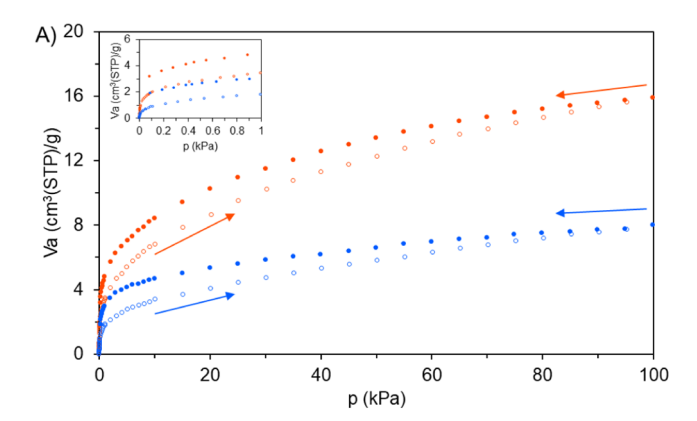


Figure 3. A) SEM and B) TEM micrographs of typical long 1DL segments. Sample was prepared by drop casting 1DL colloid onto porous alumina. 1DL slurry was washed with 0.5 M LiCl aqueous solution before drop casting.

that our material is a 1DL titanate. <sup>19,20</sup> Figure 3B shows a high-resolution TEM image of our sample. The sample possesses a wire-like structure consistent with the SEM image, and black circle regions can be observed. The circle regions have a darker color than the other regions, which suggests that the circle region has a higher electron absorption efficiency than the other regions.

Figure 4A plots the  $CO_2$  adsorption isotherm of the FD powders at 25 and 80 °C. For both temperatures, hysteresis loops were obtained. From the shape of the loops it is reasonable to conclude that the isotherms are of type IV. In other words, we are dealing with porous mesostructures. This result also indicates that once the  $CO_2$  adsorbs on the 1DL, it becomes more difficult to detach from it. The isotherms are steep in the low-pressure regime, indicating than in that region the adsorption—desorption capabilities are high.

A heat of adsorption,  $\Delta H_{\rm ads}$ , analysis was performed for the desorption/adsorption isotherms shown, respectively, in Figures S1 and S2. The analysis results, shown in Figure 4B, indicate that the  $\Delta H_{\rm ads}$  (red symbols in Figure 4B) on adsorption are lower than their desorption counterparts (blue symbols in Figure 4B). This result is consistent with the



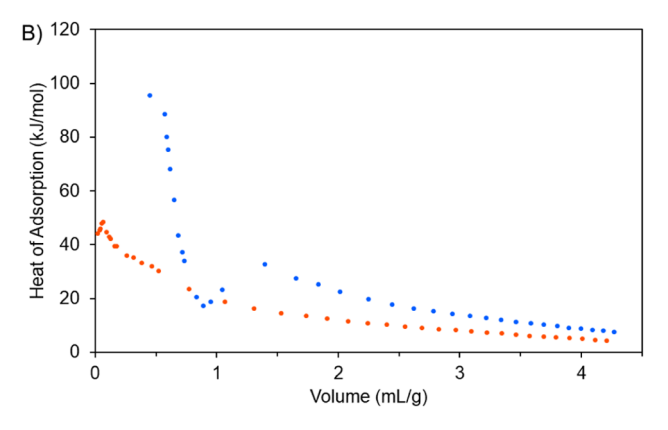


Figure 4. A) Adsorption and desorption  $\mathrm{CO}_2$  isotherms by 1DL FD powders. Red and blue plots show result at 25 and 80 °C, respectively. Data points on adsorption and desorption are shown by open and solid symbols, respectively. Inset magnifies isotherms in low-pressure region. Arrows indicate the experiment's direction. B) Heat of adsorption analysis result for  $\mathrm{CO}_2$ . Red and blue symbols represent values on adsorption and desorption, respectively.

hysteresis loops observed in Figure 4A. The fact that these heats of adsorption/desorption are unequal implies that the CO<sub>2</sub> molecules somehow interact with the 1DL surfaces. The sharp increase of adsorption volume of CO<sub>2</sub> between 273 and 278 K shown in Figures S1 and S2 indicates a change in the interaction between 1DLs and CO<sub>2</sub> molecule. The high adsorption volume suggests chemisorption of CO<sub>2</sub> at 278 K unto the 1DLs.

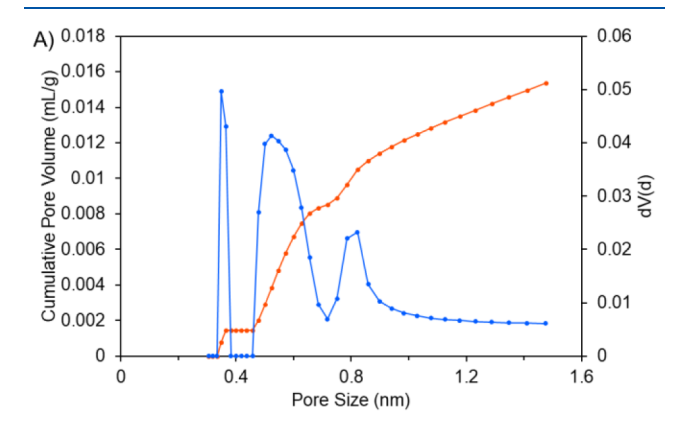
BET analysis was performed for the adsorption isotherm of  $\mathrm{CO}_2$  at 298 K (red open symbols in Figure 4A) as well as for the adsorption of  $\mathrm{N}_2$  at 77 K (Figure S3). The results are summarized in Table 1. Both gases indicate that the BET surface area obtained are comparable and relatively low. BET analysis with  $\mathrm{CO}_2$  adsorption isotherm was previously used for research on ultrasmall (<2 nm) regions because  $\mathrm{CO}_2$  can access ultramicro pores. The comparable surface areas obtained from the  $\mathrm{N}_2$  and  $\mathrm{CO}_2$  isotherms indicate that 1DLs possess ultramicro and mesopores. The theoretical surface

Table 1. Results of BET Analysis of  $N_2$  and  $CO_2$  at Different Temperatures

gas species	temp. (K)	analyzed pressure range $(p/p_0)$	BET surface area $(m^2/g)$
$N_2$	77	0.05-0.35	80.19
$CO_2$	298	0.0009-0.0054	75.60

area, assuming 2D TiO<sub>2</sub> sheets 0.5 nm thick, is  $\approx$ 500 m²/g. Recent dye adsorption experiments suggest effective SSAs of  $\approx$ 2,000 m²/g.²5 There is thus no doubt that the SSAs obtained by BET are substantially lower than the theoretical or those deduced from dye adsorption. This is not unique to 1DLs and is common in other nanomaterials such as MXenes.⁴1 The conventional wisdom here is that the N<sub>2</sub> and CO<sub>2</sub> gases only penetrate a small fraction of the pores and/or the interlayer space between the 2D layers in MXenes or the quasi-2D layers in this work.

The results of a NLDFT analysis for the  $CO_2$  adsorption/desorption isotherm of  $CO_2$  (green solid symbols in Figures S1 and 2) and  $N_2$  adsorption desorption isotherm (Figure S3) are shown in Figure 5A,B, respectively. NLDFT analysis for  $CO_2$ 



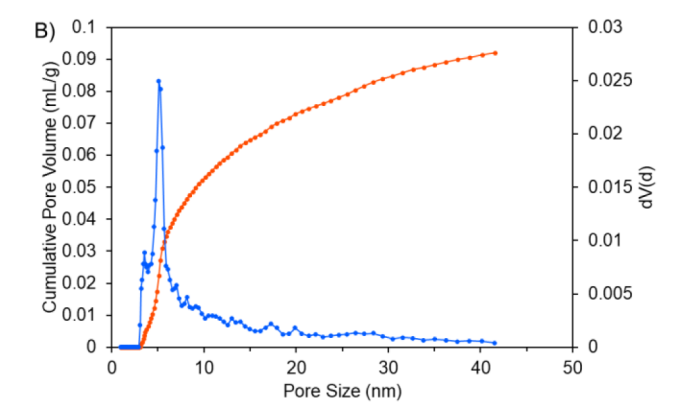


Figure 5. Pore volume vs pore width NLDFT analysis on, A) adsorption branch of the  $CO_2$  isotherm at 273 K (red solid symbols in Figures S1 and S2). B) adsorption branch of the  $N_2$  isotherm at 77 K (Figure S3). In both panels, red plots indicates cumulative pore volume; blue plot indicates pore volume for each pore diameter, dV(d).

and  $N_2$  adsorption isotherms clarifies the ultramicro and mesopore structures, respectively. When  $CO_2$  is used, the NLDFT analysis (Figure 5A) indicates that the 1DL FD powders possess three sizes of ultramicro pores, viz. 0.35 nm, 0.69 and 0.82 nm in diameter. When  $N_2$  is used on the same powder, the same analysis (Figure 5B) indicates the powder possess mesopores roughly 5 nm in diameter. It is thus reasonable to conclude that our 1DLs possess two types of pores, ultramicro and mesopores. The ultramicroporous and mesoporous volumes of the 1DL FD powders are 0.013 and 0.18, respectively, given that the BET areas for the two gases

are comparable (Table 1) it follows that a  $\approx$  6 time difference in pore volume exists.

The SSA obtained from BET analysis is almost the same, but the difference in volume is six times. This difference indicates that the smaller quantity of difference in surface area would result from the enhancement of surface area in the refinement of pores.

#### CONCLUSIONS

In summary, herein we report for the first time on the  $CO_2$  gas adsorption capacity and the pore structures of 1DL. Compared with  $TiO_2$  anatase, the  $CO_2$  adsorption capacity of 1DL (0.71 mmol/g at 298 K and 100 kPa) is more than 10 times that of anatase (0.061 mmol/g at 298 K and 100 kPa). This is likely due to the presence of the ultramicro pores in 1DLs. Moreover, 1DLs has a substantially larger  $CO_2$  adsorption capacity than that of  $Ti_3C_2$  MXene (0.18 mmol/g at 298 K and 415 kPa).

However, the mechanism by which each pore size contributes to CO<sub>2</sub> adsorption, which sites adsorb CO<sub>2</sub>, and the reason why detachment of adsorbed CO<sub>2</sub> seems more difficult remain unclear. Although there are several unknowns at this stage, the easy and industrially friendly synthesis procedure of 1DLs<sup>21,22</sup> and its unique optical properties<sup>32</sup> in that the band gap energy of bulk TiO<sub>2</sub> cannot be modified but that of 1DL TiO<sub>2</sub> can be tunable, suggest that 1DL TiO<sub>2</sub> is promising as a novel adsorbent for CO<sub>2</sub> capture and utilization applications.

#### ASSOCIATED CONTENT

#### **Supporting Information**

The Supporting Information is available free of charge at https://pubs.acs.org/doi/10.1021/acs.langmuir.4c01689.

Adsorption—desorption isotherms by 1DL FD powders ( $CO_2@$  263 K, 268 K, 273 K, 278 K, 283 K, 288 and 293 K). Adsorption desorption isotherms by 1DL FD powders ( $N_2$  at 77 K). Results of BET analysis (PDF)

#### AUTHOR INFORMATION

#### **Corresponding Authors**

Akimaro Yanagimachi — Murata Manufacturing Co., Ltd., Nagaokakyo-shi, Kyoto 617-8555, Japan; ocid.org/0009-0000-9172-1118; Email: akimaro.yanagimachi@murata.com

Takeshi Torita — Murata Manufacturing Co., Ltd., Nagaokakyo-shi, Kyoto 617-8555, Japan; Email: t\_torita@murata.com

Michel W. Barsoum — Department of Materials Science and Engineering, Drexel University, Philadelphia, Pennsylvania 19104, United States; Orcid.org/0000-0001-7800-3517; Email: barsoumw@drexel.edu

#### **Authors**

Takayuki Kono – Murata Manufacturing Co., Ltd., Nagaokakyo-shi, Kyoto 617-8555, Japan

Kota Ota – Murata Manufacturing Co., Ltd., Nagaokakyo-shi, Kyoto 617-8555, Japan

Daja R. Bonilla – Department of Chemistry & Materials Science, Fayetteville State University, Fayetteville, North Carolina 28301, United States

- Daniel E. Autrey Department of Chemistry & Materials Science, Fayetteville State University, Fayetteville, North Carolina 28301, United States
- **Hussein O. Badr** Department of Materials Science and Engineering, Drexel University, Philadelphia, Pennsylvania 19104, United States

Complete contact information is available at: https://pubs.acs.org/10.1021/acs.langmuir.4c01689

#### **Author Contributions**

The manuscript was written through contributions of all authors. All authors have given approval to the final version of the manuscript.

#### Notes

The authors declare no competing financial interest.

#### ACKNOWLEDGMENTS

D.E.A. would like to acknowledge financial support of NSF HBCU-UP RIA (HRD 1800795). M.B.W. would like to acknowledge financial support of NSF (DMR-2211319). This research was also funded by Murata Manufacturing Co., Ltd.

#### ABBREVIATIONS

1DL, one-dimensional lepidocrocite;; TiO<sub>2</sub>, titanium dioxide; FD, freeze-dried; XRD, X-ray diffraction; SEM, scanning electron microscope; HoA, heat of adsorption; NLDFT, nonlocal density functional theory; MOFs, metal—organic frameworks; TMAH, tetramethylammonium hydroxide; TiC, titanium carbide; TiB<sub>2</sub>, titanium diboride; SE, secondary electron; BET, Brunauer—Emmett—Teller

#### REFERENCES

- (1) Houghton, J. Global warming. Rep. Prog. Phys. 2005, 68, 1343-
- (2) Green Growth Strategy Through Achieving Carbon Neutrality in 2050. https://www.meti.go.jp/english/policy/energy\_environment/global\_warming/ggs2050/index.html.
- (3) van der Werf, G. R.; Morton, D. C.; DeFries, R. S.; Olivier, J. G. J.; Kasibhatla, P. S.; Jackson, R. B.; Collatz, G. J.; Randerson, J. T. CO<sub>2</sub> emissions from forest loss. *Nat. Geosci.* **2009**, *2*, 737–738.
- (4) de Kleijne, K.; Hanssen, S. V.; van Dinteren, L.; Huijbregts, M. A. J.; van Zelm, R.; de Coninck, H. Limits to Paris Compatibility of CO<sub>2</sub> Capture and Utilization. *One Earth* **2022**, *5* (2), 168–185.
- (5) Alvarado, V.; Manrique, E. Enhanced Oil Recovery: An Update Review. *Energies* **2010**, *3*, 1529–1575.
- (6) Aresta, M.; Dibenedetto, A.; Angelini, A. The Changing Paradigm in CO<sub>2</sub> Utilization. *J. CO2 Util.* **2013**, 3–4, 65–73.
- (7) Morison, J. I. L.; Lawlor, D. W. Interactions Between Increasing CO<sub>2</sub> Concentration and Temperature on Plant Growth. *Plant, Cell Environ.* **1999**, 22, 659–682.
- (8) Power, I. M.; Harrison, A. L.; Dipple, G. M.; Wilson, S.; Kelemen, P. B.; Hitch, M.; Southam, G. Carbon Mineralization: From Natural Analogues to Engineered Systems. *Rev. Mineral. Geochem.* **2013**, 77 (1), 305–360.
- (9) Wang, S.; Shi, C.; Liu, H.; Zhang, L.; Zhao, J.; Song, Y.; Ling, Z. Methionine Aqueous Solution Loaded Vermiculite/MXene Aerogels for Efficient CO<sub>2</sub> Storage via Gas Hydrate. Fuel **2023**, 334 (2), 126833.
- (10) Shen, J.; Wu, Z.; Li, C.; Zhang, C.; Genest, A.; Rupprechter, G.; He, L. Emerging applications of MXene materials in CO<sub>2</sub> photocatalysis. *FlatChem* **2021**, *28*, 100252.
- (11) Li, L.; Wang, J.; Zhang, Z.; Yang, A.; Yang, Y.; Su, B.; Bao, Z.; Ren, Q. Inverse Adsorption Separation of CO<sub>2</sub>/C<sub>2</sub>H<sub>2</sub> Mixture in Cyclodextrin- Based Metal-Organic Frameworks. *ACS Appl. Mater. Interfaces* **2019**, *11*, 2543–2550.

- (12) Gassensmith, J. J.; Kim, J. Y.; Holcroft, J. M.; Farha, O. K.; Stoddart, J. F.; Hupp, J. T.; Jeong, N. C. A Metal-Organic Framework-Based Material for Electrochemical Sensing of Carbon Dioxide. *J. Am. Chem. Soc.* **2014**, *136*, 8277–8282.
- (13) Siriwardane, R. V.; Shen, M.-S.; Fisher, E. P.; Poston, J. A. Adsorption of  $CO_2$  on Molecular Sieves and Activated Carbon. *Energy Fuels* **2001**, *15* (2), 279–284.
- (14) Shafeeyan, M. S.; Daud, W. M. A. W.; Houshmand, A.; Shamiri, A. A review on Surface Modification of Activated Carbon for Carbon Dioxide Adsorption. *J. Anal. Appl. Pyrolysis* **2010**, *89* (2), 143–151.
- (15) Mino, L.; Spoto, G.; Ferrari, A. M. CO<sub>2</sub> Capture by TiO<sub>2</sub> Anatase Surfaces: A Combined DFT and FTIR Study. *J. Phys. Chem.* C **2014**, *118*, 25016–25026.
- (16) Jitan, S. A.; Palmisano, G.; Garlisi, C. Synthesis and Surface Modification of TiO<sub>2</sub>-Based Photocatalysts for the Conversion of CO<sub>2</sub>. *Catalysts* **2020**, *10*, 227.
- (17) Michalkiewicz, B.; Majewska, J.; Kadziolka, G.; Bubacz, K.; Mozia, S.; Morawski, A. W. Reduction of CO<sub>2</sub> by Adsorption and Reaction on Surface of TiO<sub>2</sub>-nitrogen Modified Photocatalyst. *J. CO2 Util.* **2014**, *5*, 47–52.
- (18) Ola, O.; Maroto-Valer, M. M. Review of Material Design and Reactor Engineering on TiO<sub>2</sub> Photocatalysis for CO<sub>2</sub> Reduction. *J. Photochem. Photobiol., C* **2015**, 24, 16–42.
- (19) Crake, A.; Christoforidis, K. C.; Kafizas, A.; Zafeiratos, S.; Petit, C. CO 2 capture and photocatalytic reduction using bifunctional TiO 2/MOF nanocomposites under UV-vis irradiation. *Appl. Catal. B* **2017**, *210*, 131–140.
- (20) Badr, H. O.; Barsoum, M. W. Hydroxide-Derived Nanostructures: Scalable Synthesis, Characterization, Properties and Potential Applications. *Adv. Mater.* **2024**, 2402012.
- (21) Badr, H. O.; El-Melegy, T.; Carey, M.; Natu, V.; Hassig, M. Q.; Johnson, C.; Qian, Q.; Li, C. Y.; Kushnir, K.; Colin-Ulloa, E.; Titova, L. V.; Martin, J. L.; Grimm, R. L.; Pai, R.; Kalra, V.; Karmakar, A.; Ruffino, A.; Masiuk, S.; Liang, K.; Naguib, M.; Wilson, O.; Magenau, A.; Montazeri, K.; Zhu, Y.; Cheng, H.; Torita, T.; Koyanagi, M.; Yanagimachi, A.; Ouisse, T.; Barbier, M.; Wilhelm, F.; Rogalev, A.; Björk, J.; Persson, P. O. Å.; Rosen, J.; Hu, Y.-J.; Barsoum, M. W. B.-U. Bottom-up, scalable synthesis of anatase nanofilament-based two-dimensional titanium carbo-oxide flakes. *Mater. Today* **2022**, *54*, 8–17.
- (22) Badr, H. O.; Lagunas, F.; Autrey, D. E.; Cope, J.; Kono, T.; Torita, T.; Klie, R. F.; Hu, Y.-J.; Barsoum, M. W. On the Structure of One-Dimensional TiO<sub>2</sub> Lepidocrocite. *Matter* **2023**, *6* (1), 128–141.
- (23) Sudhakar, K.; Karmakar, A.; Badr, H.; El-Melegy, T.; Hassig, M. Q.; Carey, M.; Masiuk, S.; Wu, L.; Qian, Q.; Kono, T.; et al. One-Dimensional Lepidocrocite Titania Mesoparticles Integrated with Activated Carbon for High-Performance Supercapacitor Applications. *Matter* 2023, *6*, 2834.
- (24) Wang, L.; Badr, H. O.; Yang, Y.; Cope, J. H.; Ma, E.; Ouyang, J.; Yuan, L.; Li, Z.; Liu, Z.; Barsoum, M. W.; et al. Unique Hierarchical Structures of One Dimensional Lepidocrocite Titanate with Cation-Exchangeable Sites for Extraordinary Selective Actinide Capture for Water Purification. *Chem. Eng. J.* 2023, 474, 145635.
- (25) Walter, A. D.; Schwenk, G. R.; Cope, J.; Lindsay, A. J.; Sudhakar, K.; Hassig, M. Q.; Ferrer, L.; Minnini, A.; Hu, Y.-J.; Barsoum, M. W. Adsorption and Self-Sensitized Photodegradation of Rhodamine 6G and Crystal Violet by One-Dimensional Titanium Dioxide-based Lepidocrocite Under Visible Light. *Matter* 2023, 6, 4086–4105.
- (26) Ge, M.; Cao, C.; Huang, J.; Li, S.; Chen, Z.; Zhang, K.-Q.; Al-Deyab, S.; Lai, Y. A Review of One-Dimensional TiO<sub>2</sub> Nano-structured Materials for Environmental and Energy Applications. *J. Mater. Chem. A* **2016**, *4* (18), 6772–6801.
- (27) Lee, K.; Mazare, A.; Schmuki, P. One-dimensional Titanium Dioxide Nanomaterials: Nanotubes. *Chem. Rev.* **2014**, *114* (19), 9385–9454.
- (28) Kolen'ko, Y. V.; Kovnir, K. A.; Gavrilov, A. I.; Garshev, A. V.; Frantti, J.; Lebedev, O. I.; Churagulov, B. R.; Van Tendeloo, G.; Yoshimura, M. Hydrothermal Synthesis and Characterization of

- Nanorods of Various Titanates and Titanium Dioxide. J. Phys. Chem. B 2006, 110, 4030.
- (29) Schneider, C.; Liu, N.; Romeis, S.; Peukert, W.; Schmuki, P. Easy Room Temperature Synthesis of High Surface Area Anatase Nanowires with Different Morphologies. *ChemistryOpen* **2019**, *8*, 817.
- (30) Ishikawa, Y.; Tsukimoto, S.; Nakayama, K. S.; Asao, N. Ultrafine Sodium Titanate Nanowires with Extraordinary Sr Ion-Exchange Properties. *Nano Lett.* **2015**, *15* (5), 2980–2984.
- (31) Esmat, M.; Farghali, A. A.; El-Dek, S. I.; Khedr, M. H.; Yamauchi, Y.; Bando, Y.; Fukata, N.; Ide, Y. Conversion of a 2D Lepidocrocite-Type Layered Titanate into Its 1D Nanowire Form with Enhancement of Cation Exchange and Photocatalytic Performance. *Inorg. Chem.* **2019**, *58* (12), 7989–7996.
- (32) Colin-Ulloa, E.; Martin, J. L.; Hanna, R. J.; Frasch, M. H.; Ramthun, R. R.; Badr, H. O.; Uzarski, J. R.; Barsoum, M. W.; Grimm, R. L.; Titova, L. V. Electronic Structure of 1D Lepidocrocite TiO<sub>2</sub> as Revealed by Optical Absorption and Photoelectron Spectroscopy. *J. Phys. Chem. C* **2023**, *127* (15), 7275–7283.
- (33) Badr, H. O.; Cope, J.; Kono, T.; Torito, T.; Lagunas, F.; Castiel, E.; Klie, R. F.; Barsoum, M. W. Titanium Oxide-Based 1D Nanofilaments, 2D Sheets, and Mesoporous Particles: Synthesis, Characterization, and Ion Intercalation. *Matter* **2023**, *6* (10), 3538–3554.
- (34) Cardoza, N.; Badr, H. O.; Pereira, R.; Barsoum, M. W.; Kalra, V. O.-D. One-Dimensional, Titania Lepidocrocite-Based Nanofilaments and Their Polysulfide Anchoring Capabilities in Lithium—Sulfur Batteries. ACS Appl. Mater. Interfaces 2023, 15 (44), 50973—50980
- (35) Badr, H. O.; Natu, V.; Neaţu, Ş.; Neaţu, F.; Kuncser, A.; Rostas, A.; Racey, M. W.; Barsoum, M. W.; Florea, M. Photo-stable, 1D-nanofilaments TiO<sub>2</sub>-based lepidocrocite for photocatalytic hydrogen production in water-methanol mixtures. *Matter* **2023**, *6* (9), 2853–2869.
- (36) Wilson, O. R.; Carey, M. S.; Cope, J. H.; Badr, H. O.; Nantz, J. M.; ElMelegy, T. A.; Barsoum, M. W.; Magenau, A. J. D. Repairable Reinforced Composites of 1D TiO<sub>2</sub> Lepidocrocite Mesoparticles and Thiol-yne Click Networks via Alkylborane-initiated in situ Polymerization. *Cell Rep.* **2023**, *4*, 101434.
- (37) Panigraĥi, S.; Badr, H. O.; Deuermeier, J.; Martins, R.; Barsoum, M. W. Interfacial Engineering with One-Dimensional Lepidocrocite TiO<sub>2</sub> -Based Nanofilaments for High Performance Perovskite Solar Cells *ACS Nano.* **2024**
- (38) Lagunas, F.; Bugallo, D.; Karimi, F.; Yang, Y.; Badr, H. O.; Cope, J. H.; Ferral, E.; Barsoum, M. W.; Hu, Y.-J.; Klie, R. F. Ion-Exchange Effects in One-Dimensional Lepidocrocite TiO<sub>2</sub>: A Cryogenic Scanning Transmission Electron Microscopy and Density Functional Theory Study. *Chem. Mater.* **2024**, 36 (6), 2743–2755.
- (39) Kim, K. C.; Yoon, T.-U.; Bae, Y.-S. Applicability of Using CO<sub>2</sub> Adsorption Isotherms to Determine BET Surface Areas of Microporous Materials. *Microporous Mesoporous Mater.* **2016**, 224, 294–301.
- (40) Mukhtar, A.; Mellon, N.; Saqib, S.; Lee, S.-P.; Bustam, M. A. Extension of BET Theory to CO<sub>2</sub> Adsorption Isotherms for Ultramicroporosity of Covalent Organic Polymers. SN Appl. Sci. 2020, 2, 1232.
- (41) Tan, Z.; Sato, K.; Ohara, S. Synthesis of Layered Nanostructured  $TiO_2$  by Hydrothermal Method. *Adv. Powder Technol.* **2015**, 26 (1), 296–302.